Design and Modeling of a Sub-2 mm Steerable Neuroendoscopic Grasping Tool

Timothy A. Brumfiel,

Medical Robotics and Automation (RoboMed) Laboratory, Wallace H. Coulter Department of Biomedical Engineering, Georgia Institute of Technology, Atlanta, GA30332 USA.

Ronghuai Qi,

Medical Robotics and Automation (RoboMed) Laboratory, Wallace H. Coulter Department of Biomedical Engineering, Georgia Institute of Technology, Atlanta, GA30332 USA.

Coley Chapman,

George W. Woodruff School of Mechanical Engineering, Georgia Institute of Technology, Atlanta, GA30332 USA.

Asif Rashid,

George W. Woodruff School of Mechanical Engineering, Georgia Institute of Technology, Atlanta, GA30332 USA.

Shreyes N. Melkote,

George W. Woodruff School of Mechanical Engineering, Georgia Institute of Technology, Atlanta, GA30332 USA.

Joshua J. Chern,

Children's Healthcare of Atlanta, Atlanta, GA 30341 USA.

Jaydev P. Desai [Fellow, IEEE]

Medical Robotics and Automation (RoboMed) Laboratory, Wallace H. Coulter Department of Biomedical Engineering, Georgia Institute of Technology, Atlanta, GA30332 USA.

Abstract

Minimally invasive procedures, such as endoscopic third ventriculostomy (ETV), benefit from the increased dexterity and safety that surgical continuum robots can bring. However, due to their natural compliance, new compatible end-effectors, such as graspers or scissors, must be developed and their actuation must be considered when developing the robotic structures in which they are housed due to the inherent coupling that will be introduced. In this paper, we integrate a tendon-driven meso-scale grasper, with a closed configuration diameter of 1.69 mm, into a 2 degree-of-freedom (DoF) tendon-driven neurosurgical robot with an outer diameter of less than 2 mm. Furthermore, the kinematics of the grasper is validated and an analysis of the coupling between the grasper and the robotic joints is conducted in order to evaluate the design performance.

Timothy. A. Brumfiel is the corresponding author. tbrumfiel3@gatech.edu.

I. INTRODUCTION

Pediatric hydrocephalus is a procedure characterized by a buildup of cerebrospinal fluid (CSF) in the brain leading to swelling of the head and, if left untreated, can be fatal [1]. Endoscopic third ventriculostomy (ETV) is a minimally invasive treatment where a hole is created at the bottom of the third ventricle, allowing for CSF to drain [2]. Many neurosurgical procedures, such as ETV, can benefit greatly from the development of flexible robotic tools. These tools, typically machined from super elastic nitinol (NiTi), are characterized by their continuous, flexible structures that are actuated by the elastic deformation of the structure itself [3]–[6]. The development of end-effectors that are compatible with the flexible structure of a continuum robot is presented with many difficulties due to design miniaturization, modeling, and coupling between the end-effectors actuation and the tooling's joints.

Several works have aimed to develop micro-scale graspers for surgical applications, more specifically attempting to overcome challenges with miniaturization and actuation within compliant structures [7]–[11]. Many of these designs make use of tendon actuation, shape memory alloy (SMA) wires, and compliant push/pull mechanism. Orekhov *et al.* developed a 3D printed, tendon-driven grasper for a 6 DoF parallel continuum manipulator [12]. This grasper is capable of moving each grasper jaw independently over 180°. However, this grasper and manipulator have an outer diameter of 12 mm, which is too large for the minimally invasive neurosurgical procedures considered in this work. Fujisawa *et al.* developed a 4 DoF robotic forceps with an outer diameter of 3.5 mm using superelastic nitinol springs machined using electric discharge machining [13]. This mechanism provided 2 DoFs from the lateral motion of the joint and 2 DoFs from the graspers heading and opening/closing angles. Lim *et al.* [14] developed three types of magnetically-actuated forceps for neuroendoscopy. When the forceps are in a closed configuration they can be deployed through a 3.2 mm diameter working channel. However, their surgical precision, dexterity, and efficiency need to be improved. Craker *et al.* [15] proposed an SMA-driven grasper. This grasper (3 mm OD) has a fixed jaw and an actuated jaw attached to a flexible joint. By pulling a tendon on the actuated jaw, the flexible joint bends and the actuated jaw closes on the fixed jaw. But this grasper has limited workspace because it only has one actuated jaw. Dimitrakakis *et al.* [16] developed a handheld robotic instrument for minimally invasive neurosurgery, where the 3-DoF tendon-driven robotic end-effector attached to the distal tip of this instrument consists of a spherical joint and a grasper. However, this grasper has one actuated jaw and an outer diameter of 4 mm. Table I includes a comparison of surgical grasping tools developed including their actuation modality, structure type (compliant or rigid linkages), and intended tool structure (commercial rigid device or steerable tool).

In this paper, we detail the design and fabrication of a 2 DoF, tendon-driven, steerable robotic tool with a small-scale tendon-driven grasper, breifly introduced in [17], integrated into the tip in which the entire assemble has an outer diameter of less than 2 mm, capable of fitting within the working channel of commercial endoscopic working channels. Furthermore, we analyze the grasper kinematics and the coupling between the motion of the grasper for use in future works toward fully automating the motion of the robotic tool.

The paper is organized as follows. First in Section II we detail the design and fabrication of the steerbale joint (Section II-A), the robotic grasper (Section II-B), its actuation system (Section II-C), and produce the mapping between the tendon stroke and grasper angle (Section II-D). In Section III we validate the kinematics of the grasper (Section III-A) and experimentally quantify the coupling between the graspers motion and the steerable joint (Section III-B). Section IV provides a discussion of the results. Lastly, in Section V we detail our conclusion and future directions.

II. MECHANISM DESIGN

A. Steerable Joint

The steerable endoscopic tool shown in Fig.1(a), modified from our previous work [6], consists of two compliant joints. Each joint is machined from a single nitinol tube (OD: 1.93 mm and ID: 1.44 mm) using a femtosecond laser (WS-Flex Ultra-Short Pulse Laser Workstation, Optec, Frameries, Belgium). The proximal joint has a rectangular unidirectional asymmetric notch pattern machined into the base where each of the notches have width, spacing in between, and depth of cut (defined as the % of the diameter removed) are 0.5 mm, 0.2 mm, and 82%, respectively. At the top of the proximal joint, a small channel has been etched into the tube with small rectangular cuts at the ends where a 0.152 mm diameter nitinol wire (McMaster-Carr®, GA, USA) is soldered. Applying tension to each of the tendons generates a deflection in the respective joint.

The distal joint of the robot consists of a rectangular bidirectional asymmetric notch pattern where each notch's width, spacing, and depth of cut are 0.5 mm, 0.235 mm, and 82%, respectively. The distal joint of the robot is significantly more compliant than the proximal joint due to the bidirectional notch pattern and chosen cutting parameters. This allows for minor coupling to have minimal impact on joint motion as the proximal joint requires approximately 4x the force to achieve the same deflection angle as the distal joint. Similar to the proximal joint, the distal joint's 0.076 mm tendon is soldered to an etched area on the distal end of the joint. This tendon is routed through two steel plates on the body, shown in Fig.1(a)(left inset), used to separate the joint and grasper tendons and to partially constrain the distal joint's tendon to lie along the proximal joint's neutral axis to eliminate coupling between the joints as much as possible. The combination of routing through the neutral axis and the increased stiffness of the proximal nearly isolates each joint's motion. At the base of the robot, a 3D printed component (Projet 5600, 3D Systems, South Carolina, USA) is used to attach the robot to an approximately 25cm channel made of stainless steel with an OD of 1.96 mm.

B. Robotic Grasper

The robotic grasper, shown in Fig.1(a)(right inset), consists of a scissor linkage system driven by an input linkage through the use of a 0.076 mm OD nitinol tendon. Each grasper jaw is machined from 1.5 mm thick 316L stainless steel sheets using a 5-axis CNC micromill (CNC MiniMill/GX, Minitech Machinery Corp., GA, USA). The steel sheets are secured to a Delrin block and machined at spindle speeds ranging from 10k-55k RPM with

micro end mills of diameters 0.3–1.0 mm. Each of the grasper's components are then taken to a femtosecond laser for deburring and fine tuning some of the components dimensions.

Connected to each of the graspers is an intermediate linkage. These linkages are machined from 0.4 mm thick 316L stainless steel sheets and have a width and length of 0.6 mm and 1.6 mm, respectively. The intermediate linkages contain a small step on the side facing away from the grasper to ensure the complete assembly interfaces properly without significant play in the joints. These linkages are attached to the grasper through an extrusion on the grasper's base that contains a small step which allows for a stainless steel cap of thickness 0.2 mm to be soldered on, thus constraining the intermediate linkages laterally.

The ends of the intermediate linkages are attached to the input linkage. This linkage is machined on the femtosecond laser from 0.4 mm thick stainless steel and has a length and width of 3 mm and 0.6 mm, respectively. This linkage and the two intermediate linkages from the graspers are secured using a nitinol tube with a 0.3 mm OD which has been plastically deformed on each end in order to constrain the far end of the assembly laterally. A nitinol tendon with a diameter of 0.076 mm is attached to the input linkage by looping the tendon through the linkage and crimping it through the use of a 0.2 mm OD nitinol tube secured on each ends with solder. The robotic grasper prior to assembly within the joint is shown in shown in Fig.1(b).

The input linkage of the assembly is encapsulated by a compression spring with a stiffness of 0.24 N/mm, resting length of 2 mm, and maximum compression of 1.47 mm. This assembly is placed into the distal end of the tube. The spring is compressed against two 0.3 mm nitinol pins that are soldered in place and the grasper is secured through the main shaft at the far end of the tube which is a 0.3 mm nitinol wire. To constrain the grasper laterally at the tip of the robot, two nitinol tubes (OD: 0.48 mm and ID: 0.4 mm) are used as collars to press the grasper inward, secured on the outer surface by solder. The grasper's tendon is then routed throughout the body and 3D printed routing blocks toward the actuation system. The steerable tool is shown in Fig.1(c) where a zoom in of the linkages and compression spring mechanism can be seen in Fig.1(c)(inset).

C. Actuation System

Each of the robot's joints and the robotic grasper are actuated by nitinol tendons. These tendons are routed through small pulley assemblies and are actuated through the use of a 3D printed actuation system shown in Fig.2(a) along with the robotic tip in Fig.2(a)(inset). The actuation system consists of 3 brushed DC motors (Maxon Precision Motors, MA, USA), shown in Fig.2(b), with a 0.5 mm pitched lead screw attached. Each of these motors are responsible for bending the proximal and distal joints, denoted by θ_1 and θ_2, respectively, and actuating the grasper. This assembly is encapsulated in a 3D printed housing held inside two bearings. A DC motor (Pololu Robotics and Electronics, NV, USA) is attached to a 2:1 gear reduction on the backend to rotate the steerable tip by an angle ϕ. Lastly, a DC motor and 0.5 mm pitch lead screw along with linear rails is used to translate the robot by a distance d. Each tendon is routed through a small 3D-printed pulley at the front of the actuation system as shown in Fig.2(b)(inset). A picture of the actuation system is shown in Fig.2(c). The degrees-of-freedom of the system are summarized as follows:

$$\begin{bmatrix} d \\ \phi \\ \theta_1 \\ \theta_2 \\ \varphi \end{bmatrix} = \begin{bmatrix} \text{Tool Insertion} \\ \text{Tool Rotation} \\ \text{Proximal Bending Angle} \\ \text{Distal Bending Angle} \\ \text{Grasper Angle} \end{bmatrix}$$

D. Grasper Kinematics

The grasper kinematics is a mapping of the input tendon stroke, t_g, to the grasping angle, denoted as φ. When the grasper is completely open ($t_g = 0$) there is a distance between the axis of rotation of the graspers and the previous joining of linkages denoted as x_0 as shown in Fig. 3(a-1). The grasper angle can be determined through the mapping:

$$\varphi = 2\arccos\left(\frac{(x + x_0)^2 + L_2^2 - L_1^2}{2(x + x_0)L_2}\right) - 2\psi$$

(1)

and therefore, the desired motion for some angle can be given as:

$$x = L_2\cos\left(\frac{\varphi}{2} + 2\psi\right) + \sqrt{L_1^2 - L_2^2\sin^2\left(\frac{\varphi}{2} + 2\psi\right)} - x_0$$

(2)

Where ψ is an angle constant offset between the jaws and linkages, L_1 is the center-to-center distance between the intermediate linkages holes, L_2 is the distance between the fixed axis on the jaws and the joining with L_1, and x is how much the input linkage has moved as shown in Fig.3(a-2). In the case where the joint is not bent, the elongation is easily quantified and the transmitted motion can be given as:

$$t_g = x + \frac{KLx}{E\pi r^2} = \left(1 + \frac{KL}{E\pi r^2}\right)x$$

(3)

Where K is the spring stiffness, E is the Young's modulus of the nitinol tendon, L is the original length of the tendon, and r is the radius of the nitinol tendon. These values can be measured to adequate precision such that grasper parameters are only considered while calibrating the kinematics.

III. EXPERIMENTAL RESULTS AND DISCUSSION

A. Kinematic Calibration—Although the parameters of the linkages are known from high-precision machining, once assembled, due to small tolerances in the axes of rotation due to assembly errors, the known distances of the assembly are slightly incorrect, leading to large errors in the predicted joint values. To calibrate these values, the grasper tendon was loaded quasistatically in the home configuration with a CMOS camera (CS165MU/M,

Thorlabs, Newton, NJ) imaging the plane in which the graspers open (Fig.3(b-1)) and close Fig.3(b-2). These images were gathered as the tendon stroke values are recorded. For each camera frame, a Hough transform was conducted on each of the grasper jaws using the Matlab® Image Processing Toolbox™ (MathWorks, Natick, MA, USA) in order to fit a line to the skeletonized image of each jaw which allows for the grasper angle to be computed by taking its dot product with a known zero line as shown in Fig. 3(b-1)(inset). These angles computed can be compared the tendon stroke estimated using known parameters of the nitinol tendon where tendon radius is measured as $r = 38$ μm, the original tendon length is approximately $L = 300$ mm, and the Young's modulus of the tendon, determined through tensile testing (Instron 5967 Mechanical Tester, INSTRON, MA, USA) to be approximately $E = 34.8$ GPa$\pm$7.32 MPa. The remaining distance parameters L_1 and L_2 are refined using the Matlab® Optimization Toolbox™ (MathWorks, Natick, MA, USA) with lower and upper bounds on each parameter within 10% of their original values (~0.1 mm max adjustment). Fig. 3(c-1) shows the estimated input linkage motion compared to the motor motion while Fig. 3(c-2) shows the corresponding measured grasper angle values and model predictions. The model was able to predict the grasper angle with a maximum error of 5.22°.

B. Coupling Evaluation—In order to evaluate the coupling between the joints and the grasper, which can be complex to avoid for continuum structures, the robot is moved to different configurations. This consists of proximal and distal joint actuation separately as well as the combination of both. At each point, the grasper tendon is closed using 0.1 mm increments when close to the jaws touching, in order to see what the effects of opening and closing the graspers are on the robot joints. The robot is viewed above with a CMOS camera perpendicular to the bending plane of the robot, using copy paper as a backround to aid in image processing, in order to capture the joint deflections at each configuration. For each configuration, an image was captured before and after the grasper was closed in order to evaluate how much the actuation of the grasper would influence the joint positions of both the proximal and distal joints. For each image, the Hough transform was used on the straight segments immediately following the proximal joint, and immediately following the distal joint to measure each of the joint deflections by fitting a line to each side of the joint and averaging them in order to compute the joint angles.

For each of the 35 configurations tested, no notable coupling was noticed and each angle computed by the Hough transform of each joint's edge showed no change. This is shown in Fig. 4 where the before and after photos are overlayed over one another where the standard grey-scale image indicates agreement between the images, a green hue indicates the grasper prior to being actuated, and a magenta hue indicates the steerable tool's configuration after closing the grasper.

IV. Discussion

The model is able to predict the grasper angle to an acceptable accuracy. However, the large number of parts included in the assembly, many sub-millimeter, is hypothesized to be the main source of errors. Due to the small scale achieved, reduction of the number of parts through the design of compliant grasper joints greatly reduces the grasper force able to be achieved (currently able to achieve 0.25 N [17]). Additionally, a compliant design

is hypothesized to increase motion coupling between the grasper and joint designs. Future works will explore mechanisms capable of reducing the number of components in the grasper.

It is observed that the motion between the grasper and the robot joints are almost completely decoupled. The actuation of the grasper primarily results in compression of the distal joint at higher bending angles. This compression can be reduced through the use of a, for example, rectangular bidirectional symmetric notch (BSN) pattern while maintaining the lateral stiffness of the distal joint to keep the two joints effectively decoupled.

V. CONCLUSION

In this work, a meso-scale, tendon-driven grasper was integrated into a meso-scale 2 degree-of-freedom steerable continuum joint. The grasper kinematics was evaluated and calibrated showing errors up to 5.22° in predictions generated from tendon stroke accounting for tendon elongation. Additionally, the coupling between the grasper and two steerable joints was analyzed indicating negligible motion coupling for the range of configurations conducted. Future works will focus on refining the housing for the grasper to reduce linkage misalignment that result in increased friction and slight lateral motion that can impede proper grasping. Furthermore, detailed modeling of the joint and grasper motion will be conducted to improve automated manipulation tasks through motion controller developments.

Acknowledgments

REFERENCES

[1]. Kulkarni AV, Drake JM, Mallucci CL, Sgouros S, Roth J, and Constantini S, "Endoscopic third ventriculostomy in the treatment of childhood hydrocephalus," The Journal of Pediatrics, vol. 155, no. 2, pp. 254–259.e1, 2009.

[2]. Demerdash A, Rocque BG, Johnston J, Rozzelle CJ, Yalcin B, Oskouian R, Delashaw J, and Tubbs RS, "Endoscopic third ventriculostomy: A historical review," British Journal of Neurosurgery, vol. 31, no. 1, pp. 28–32, 2017. [PubMed: 27774823]

[3]. Ball T, González-Martínez J, Zemmar A, Sweid A, Chandra S, VanSickle D, Neimat JS, Jabbour P, and Wu C, "Robotic applications in cranial neurosurgery: Current and future," Operative Neurosurgery, vol. 21, no. 6, pp. 371–379, 2021. [PubMed: 34192764]

[4]. Zeng W, Yan J, Yan K, Huang X, Wang X, and Cheng SS, "Modeling a symmetrically-notched continuum neurosurgical robot with non-constant curvature and superelastic property," IEEE Robotics and Automation Letters, vol. 6, no. 4, pp. 6489–6496, 2021.

[5]. Chitalia Y, Jeong S, Deaton N, Chern JJ, and Desai JP, "Design and kinematics analysis of a robotic pediatric neuroendoscope tool body," IEEE/ASME Transactions on Mechatronics, vol. 25, no. 2, pp. 985–995, 2020.

[6]. Chitalia Y, Jeong S, Yamamoto KK, Chern JJ, and Desai JP, "Modeling and control of a 2-dof meso-scale continuum robotic tool for pediatric neurosurgery," IEEE Transactions on Robotics, vol. 37, no. 2, pp. 520–531, 2021.

[7]. Thomas TL, Kalpathy Venkiteswaran V, Ananthasuresh GK, and Misra S, "Surgical Applications of Compliant Mechanisms: A Review," Journal of Mechanisms and Robotics, vol. 13, no. 2, 01 2021.

[8]. Aguirre M, Steinórsson ÁT, Horeman T, and Herder J, "Technology demonstrator for compliant statically balanced surgical graspers," Journal of Medical Devices, vol. 9, no. 2, 2015.

[9]. Jovanova J, Nastevska A, Frecker M, and Aguirre ME, "Analysis of a functionally graded compliant mechanism surgical grasper," in 2018 International Conference on Reconfigurable Mechanisms and Robots (ReMAR), 2018, pp. 1–8.

[10]. Hong MB and Jo Y-H, "Design and evaluation of 2-dof compliant forceps with force-sensing capability for minimally invasive robot surgery," IEEE Transactions on Robotics, vol. 28, no. 4, pp. 932–941, 2012.

[11]. Forbrigger C, Lim A, Onaizah O, Salmanipour S, Looi T, Drake J, and Diller ED, "Cable-less, magnetically driven forceps for minimally invasive surgery," IEEE Robotics and Automation Letters, vol. 4, no. 2, pp. 1202–1207, 2019.

[12]. Orekhov AL, Bryson CE, Till J, Chung S, and Rucker DC, "A surgical parallel continuum manipulator with a cable-driven grasper," in 2015 37th Annual International Conference of the IEEE Engineering in Medicine and Biology Society (EMBC), 2015, pp. 5264–5267.

[13]. Arata J, Fujisawa Y, Nakadate R, Kiguchi K, Harada K, Mitsuishi M, and Hashizume M, "Compliant four degree-of-freedom manipulator with locally deformable elastic elements for minimally invasive surgery," in 2019 International Conference on Robotics and Automation (ICRA), 2019, pp. 2663–2669.

[14]. Lim A, Schonewille A, Forbrigger C, Looi T, Drake J, and Diller E, "Design and comparison of magnetically-actuated dexterous forceps instruments for neuroendoscopy," IEEE Transactions on Biomedical Engineering, vol. 68, no. 3, pp. 846–856, 2021. [PubMed: 32746054]

[15]. Craker R, Johnson BV, Sakthivel H, and Cappelleri DJ, "Design of a Miniaturized Actuation System for Robotic Lumbar Discectomy Tools," in International Design Engineering Technical Conferences and Computers and Information in Engineering Conference, vol. Volume 10: 44th Mechanisms and Robotics Conference (MR), 08 2020.

[16]. Dimitrakakis E, Aylmore H, Lindenroth L, Dwyer G, Marcus HJ, and Stoyanov D, "Towards a handheld robotic instrument for minimally invasive neurosurgery," in Conference on New Technologies for Computer and Robot Assisted Surgery, 2022, pp. 1–2.

[17]. Brumfiel TA, Yamamoto KK, Rashid A, Shigematsu A, Chapman CH, Melkote S, Chern JJ, and Desai JP, "Design of a mesoscale grasper for robotic pediatric neuroendoscope tool," Proceedings of The 14th Hamlyn Symposium on Medical Robotics 2022, 2022.

[18]. Huan Yu and Tamadon Izadyar and Scatena, Cristianand Cela, Vitoand Naccarato, Antonio Giuseppe and Menciassi, Arianna and Sinibaldi, Edoardo, "Soft Graspers for Safe and Effective Tissue Clutching in Minimally Invasive Surgery," IEEE Transactions on Biomedical Engineering, vol. 68, no. 1, pp. 56–67, 2021. [PubMed: 32746010]
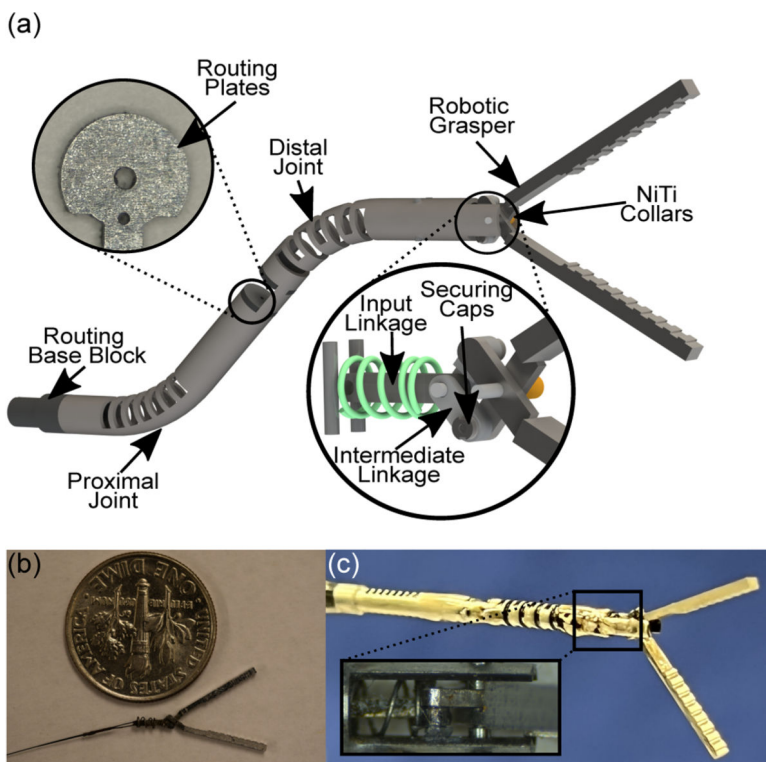
Fig. 1:
Schematic showing (a) the steerable robotic assembly with routing blocks (a)(left inset) and the internal workings of the grasper assembly (a)(right inset). A picture of (b) the grasper assembly prior to placement in the joint and (c) the final steerable robotic endoscope with (c)(inset) a zoom in of the grasper's spring mechanism.
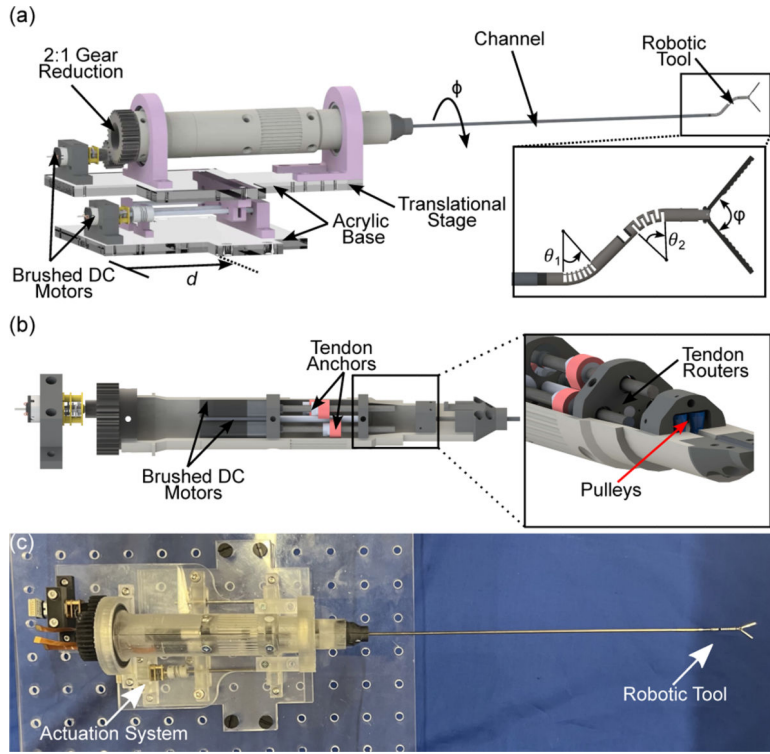
Fig. 2:
A rendering of (a) the actuation system for the robotic endoscope and grasping including the translational and rotational degrees-of-freedom along with those provided by the tool (a) (inset), (b) the internals of the actuation assembly showing each of the lead screw assemblies for tendon actuation and (b)(inset) the pulleys and holes used for routing the tendons. A picture (c) of the finalized actuation system.
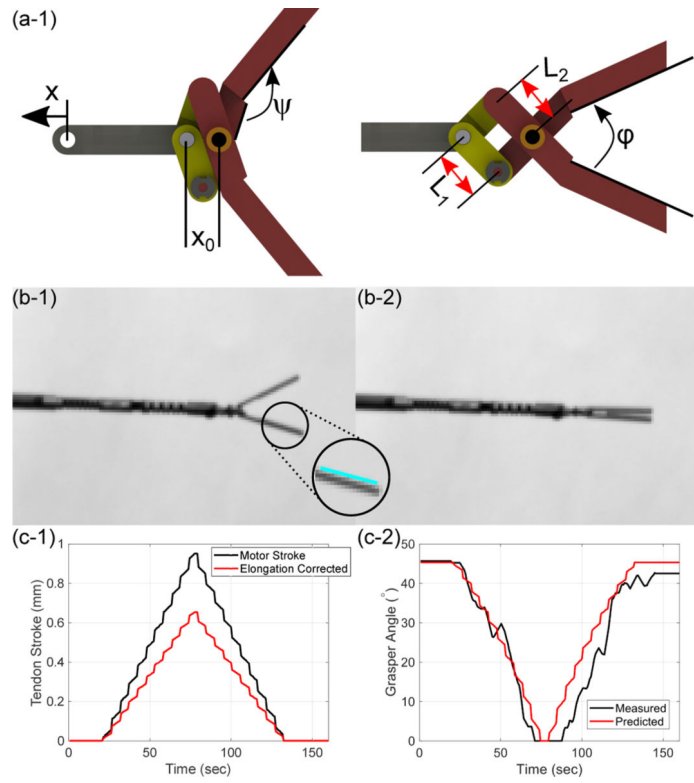
Fig. 3:
A schematic of (a-1) the grasper in its open configuration with relevant link parameters and joint angle offsets and (a-2) the actuated grasper. Pictures gathered throughout calibration of the grasper where (b-1) shows the grasper in an open configuration, (b-1)(inset) shows a sample of the hough transform lines utilized for determining the grasper configuration, and (b-2) the grasper in a closed configuration. (c-1) shows the tendon actuation compensated for tendon elongation and (c-2) the results of calibrating the model parameters to determine the grasper angle from tendon stroke data.
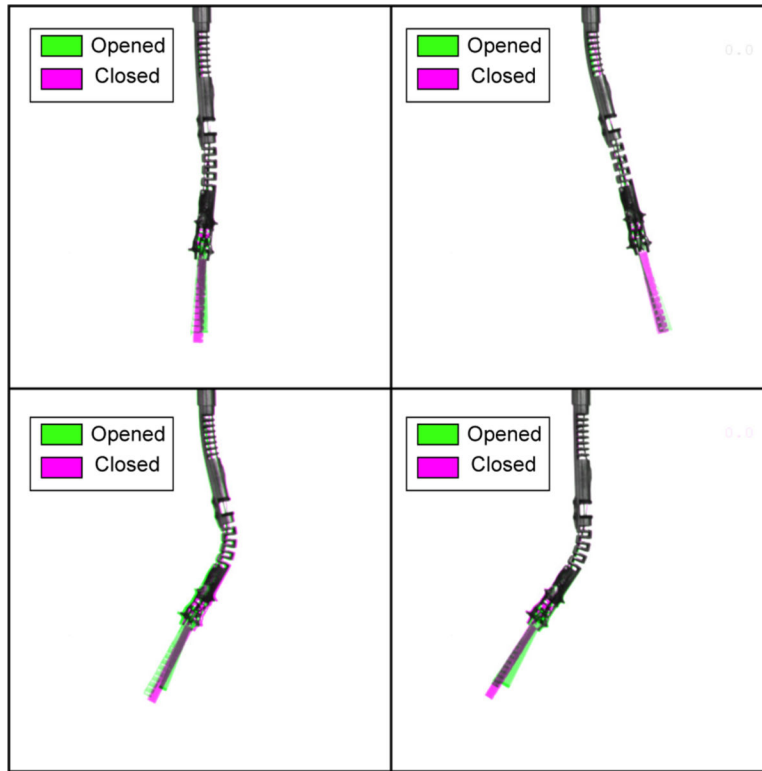
Fig. 4:
Images showing overlapped images of various configurations while opening (green hue) and closing (magenta hue) the grasper.

TABLE I:

Comparison of relevant grasper literature

Author	Year	Outer Diameter	Actuation Method	Structure Type	Intended Tool Structure
Brumfiel et al. [17]	**2022**	**1.69 mm**	**Tendon Driven**	**Rigid**	**Steerable**
Arata et al. [13]	2019	3 mm	Push/pull Springs	Compliant	Rigid
Craker et al. [15]	2020	3 mm	SMA Springs	Compliant	Rigid
Hong et al. [10]	2012	>3 mm	Tendon Driven	Compliant	Rigid
Lim et al. [14]	2021	3.2 mm	Magnetically Actuated	Compliant	Rigid
Forbrigger et al. [11]	2019	4 mm	Magnetically Actuated	Compliant	Not Specified
Aguirre et al. [8]	2015	5 mm	Push/pull rods	Compliant	Rigid
Jovanova et al. [9]	2018	5 mm	Push/pull rod	Compliant	Not Specified
Huan et al. [18]	2021	10 mm	Push/pull Rods	Rigid	Rigid
Orekhov et al. [12]	2015	12 mm	Tendon Driven	Rigid	Steerable